Supplementary Materials

Flexibility of Metal-Organic Framework Tunable by Crystal Size at the Micrometer to Submillimeter Scale for Efficient Xylene Isomer Separation

Xiao Yang, Hao-Long Zhou, Chun-Ting He, Zong-Wen Mo, Jia-Wen Ye, Xiao-Ming Chen, and Jie-Peng Zhang*

MOE Key Laboratory of Bioinorganic and Synthetic Chemistry, School of Chemistry, Sun Yat-Sen University, Guangzhou 510275, China

*zhangjp7@mail.sysu.edu.cn

Table of Contents

References

Table S1. Crystal-size dependent framework flexibility reported for MOFs.

MOF	crystal size range	Downsizing effect	reference
$[Cu_2(pypz)_2]$	500 μm ~ 1 μm	The phase transition temperature from the metastable guest-free phase (**B**) to the stable guest-free phase (**C**) increases.	This work
MAF-4 (ZIF-8)	15.8 μm ~ 10 nm	The second step of gas adsorption isotherm starts at higher pressure.	[1, 2]
DUT-49	4.08 μm ~ 100 nm	The pressure amplifications in the *n*-butane and N_2 adsorption isotherms gradually vanish.	[3]
$[Cu_2(bdc)_2(bpe)]$	700 nm ~ 50 nm	The guest removal-induced open to close framework shrinkage gradually vanishes.	[4]
DUT-8(Ni)	500 nm	The guest removal-induced open to close framework shrinkage vanishes.	[5]
$[Cu_2(bdc)_2(bpy)]$	160 nm ~ 50 nm	The guest removal-induced open to close framework shrinkage gradually vanishes.	[4]
$[Pt(CN)_4Fe(py)_2]$	16 nm	From no adsorption to gate-opening behavior.	[6]

Table S2. Crystallographic data and structure refinements.

compound	**A**	**B**	**C**
formula	$C_{20}H_{17}Cu_2N_6$	$C_{16}H_{12}Cu_2N_6$	$C_{16}H_{12}Cu_2N_6$
FW	468.47	415.40	415.40
T (K)	150(2)	150(2)	150(2)
space group	$P2_1/c$	$P2_1/c$	$P2_1/c$
a (Å)	5.71894(10)	5.3901(3)	5.2359(1)
b (Å)	20.3635(3)	20.5512(6)	15.3176(5)
c (Å)	15.3915(2)	15.2289(6)	19.5258(6)
$\beta/(°)$	94.0980(14)	98.504(4)	93.307(3)
$V/(Å^3)$	1787.88(5)	1668.4(1)	1563.37(8)
Z	4	4	4
D_c/g cm^{-3}	1.740	1.654	1.765
μ (mm^{-1})	3.085	3.218	3.435
reflns coll.	15562	12581	10113
unique reflns.	3686	3059	2755
R_{int}	0.0180	0.0478	0.0867
R_1 ($> 2\sigma(I)$) [a]	0.0279	0.0643	0.0669
wR_2 ($> 2\sigma(I)$) [b]	0.0779	0.2005	0.1700
R_1 (all data) [a]	0.0292	0.0724	0.0859
wR_2 (all data) [b]	0.0843	0.2103	0.1854
GOF	1.022	1.094	1.055

[a] $R_1 = \sum||F_o|-|F_c||/\sum|F_o|$, [b] $wR_2 = [\sum w(F_o^2-F_c^2)^2/\sum w(F_o^2)^2]^{1/2}$

Table S3. Comparison of pX adsorption selectivities reported for MOFs.

MOF	α_{pXoX}	α_{pXmX}	$\alpha_{pX/(oX + mX)}$	component	reference
3C	53.9	48.9	51.3	ternary	This work
3B	17	15	16	ternary	This work
1B	16	14	15	ternary	This work
$Ag_4(O_2CCF_3)_4(phen)_3$	9.13[a]	14.2[a]	NA	binary	[7]
Cu(CDC)	10	7	NA	binary	[8]
[Nd(HTCPB)]	NR	6.33	NA	binary	[9]
[Ce(HTCPB)]	5.65	4.55	NA	binary	[9]
MIL-125(Ti)_NH_2	2.2	4.4	NA	binary	[10]
MIL-125(Ti)	NR	3.5	NA	binary	[10]
[Zn(μ_4-L)]	3.2	2.7	2.9	ternary	[11]
MAF-4 (ZIF-8)	3.1	NR	NA	binary	[12]
CAU-1(Al)-NH_2	NR	2.8	NA	binary	[10]
MIL-140B	1.8	1.6	1.7	quaternary	[13]
MOF-48	1.7	1.7	1.7	quaternary	[13]

[a] This is not adsorption selectivity. The guests were included during the synthesis of the framework.

NR: Not reported

NA: Not available

phen = phenazine

H_2CDC = *trans*-1, 4-cyclohexanedicarboxylic acid

H_2TCPB = 4',5'-bis(4-carboxyphenyl)-[1,1',2',1''-terphenyl]-4,4''-dicarboxylic acid

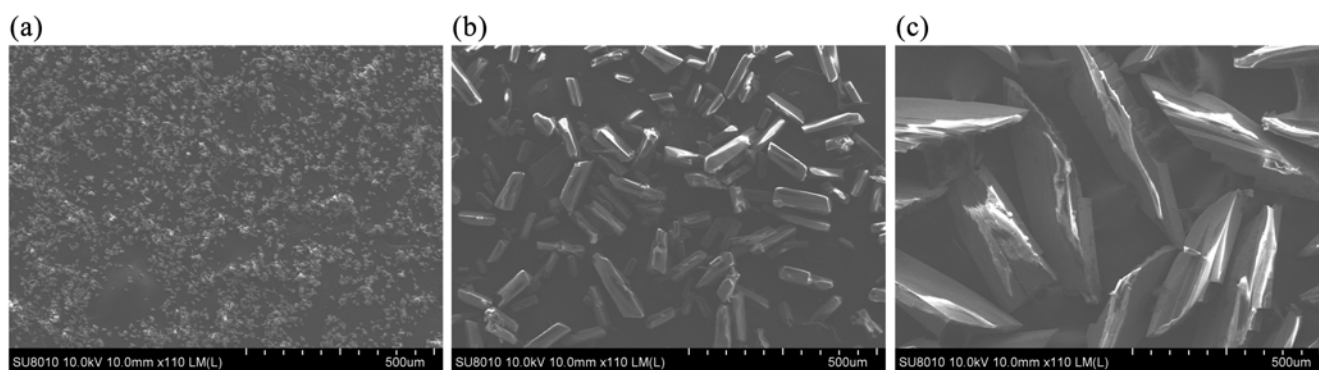H_2L = biphenyl-3,5-dicarboxylic acid

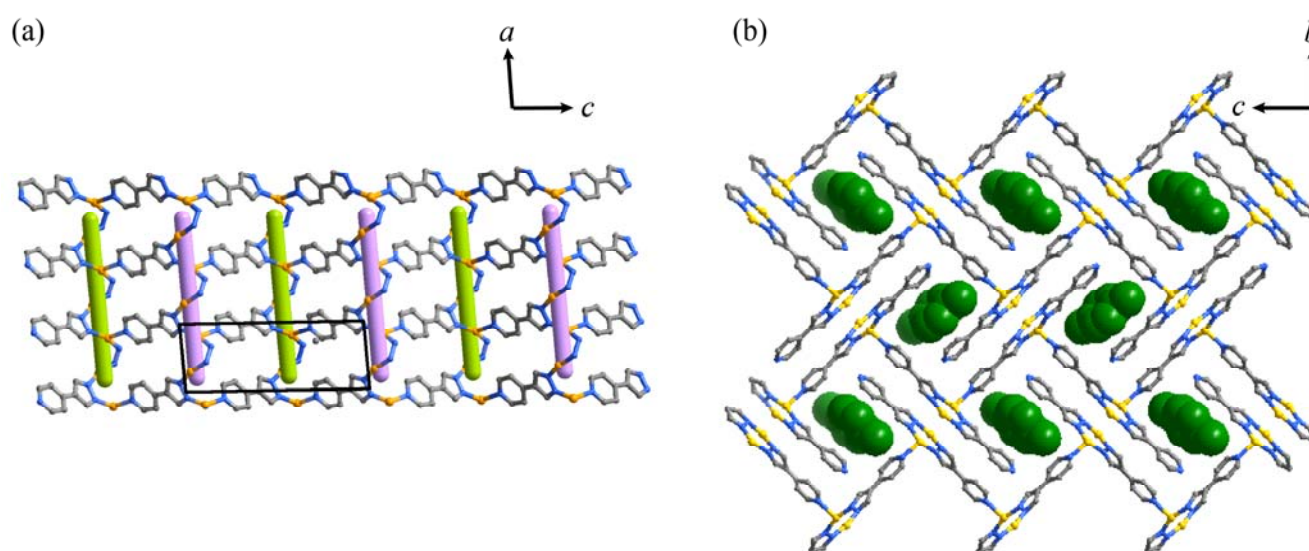**Figure S1.** SEM images of **A**. (a) **1**, (b) **2**, and (c) **3**.

Figure S2. Crystal structure of **A**: (a) a zigzag coordination layer (adjacent helical chains are highlighted in olive and violet); (b) the packing structure along the channel direction (*p*-xylene molecules are shown in space-filling mode and highlighted in green).
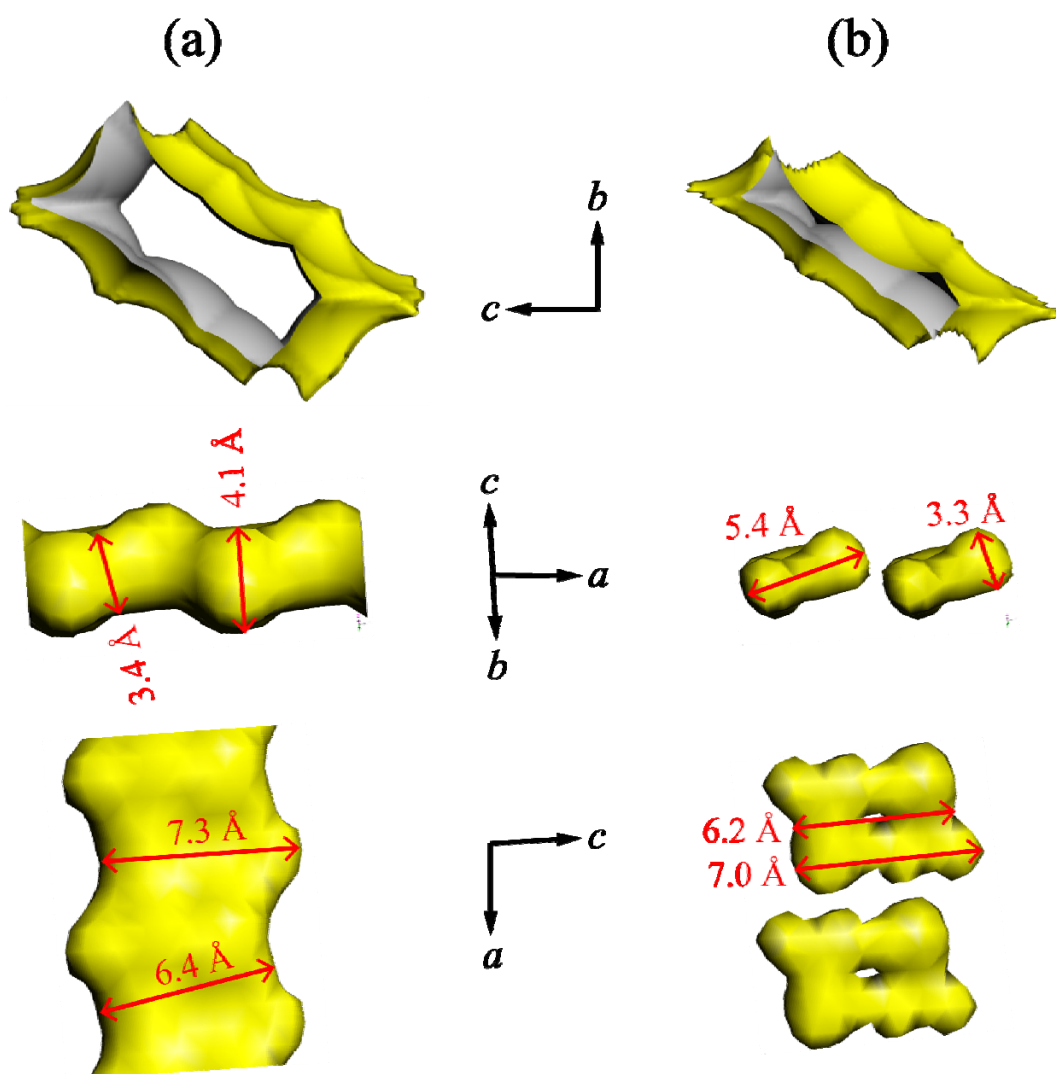
Figure S3. Detailed pore structures of (a) **A** and (b) **B** viewing along three typical directions (the pores shown in the top pannels have are shown in the same direction as in Figure 3).
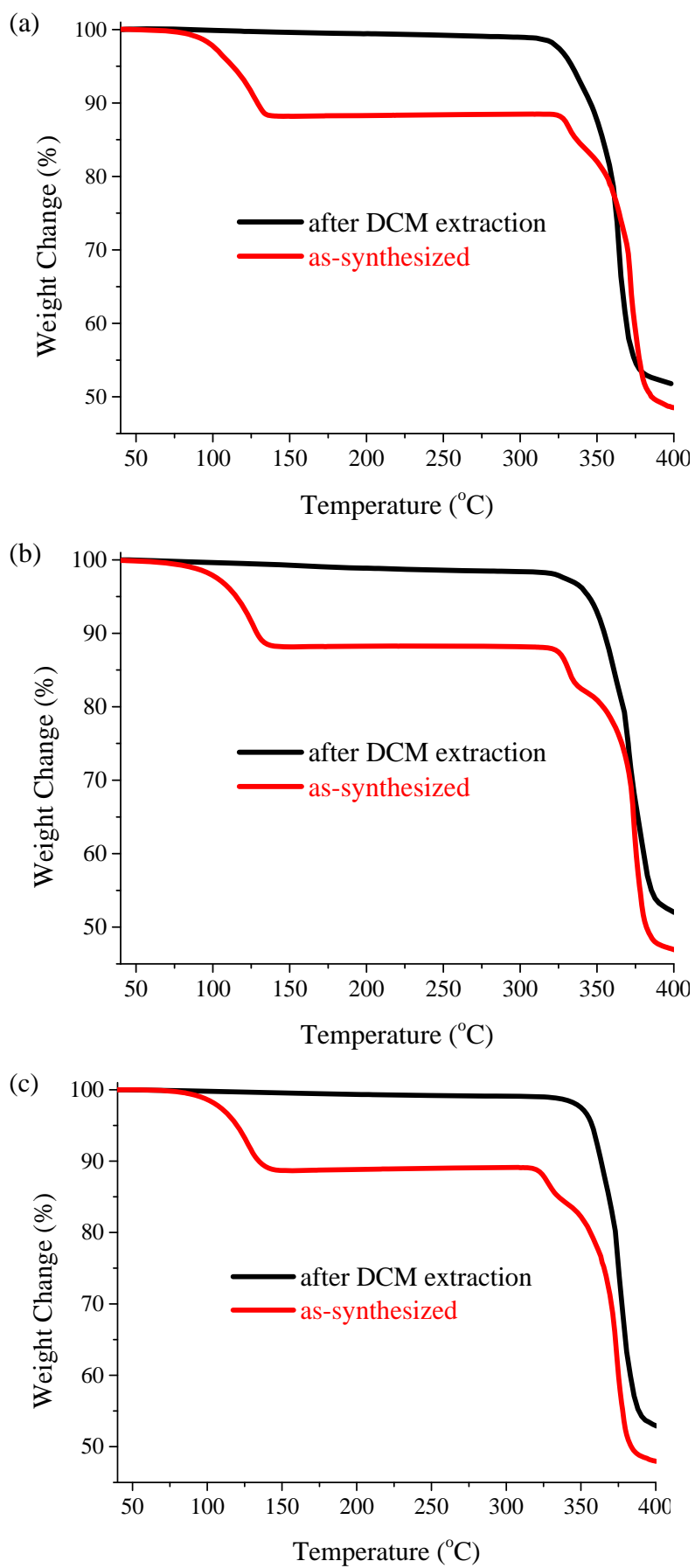
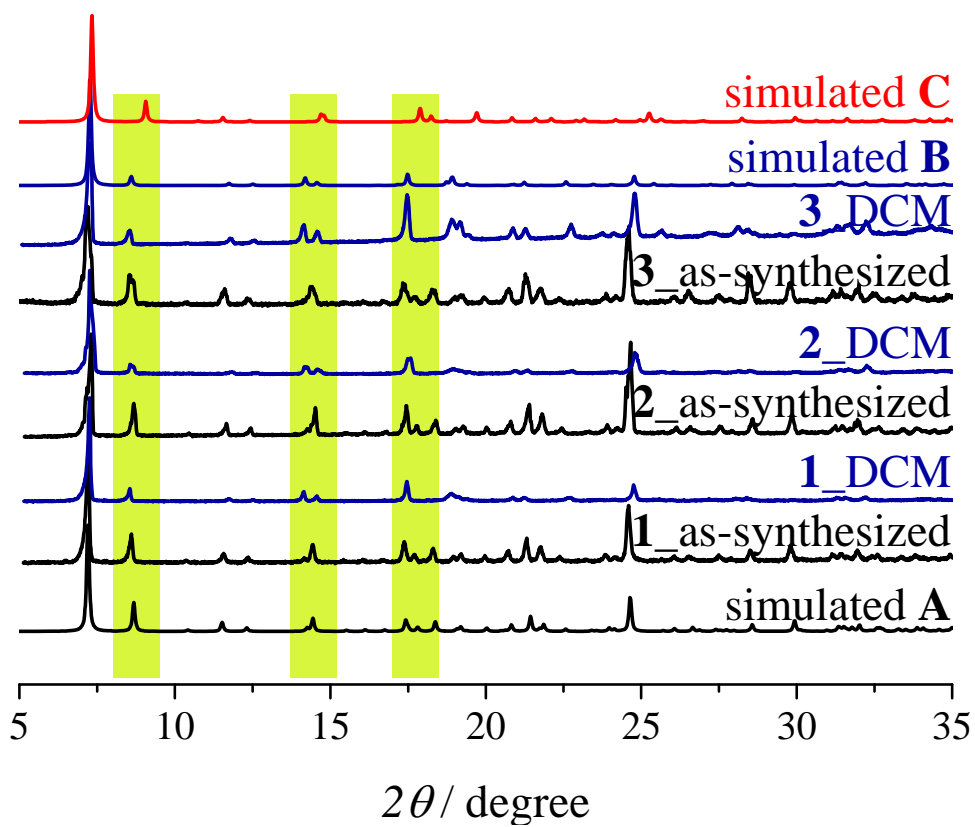**Figure S4**. TG curves of (a) **1**, (b) **2**, and (c) **3**.

Figure S5. PXRD patterns of $[Cu_2(pypz)_2] \cdot 0.5pX$ (**1**, **2**, **3**) after DCM extraction.

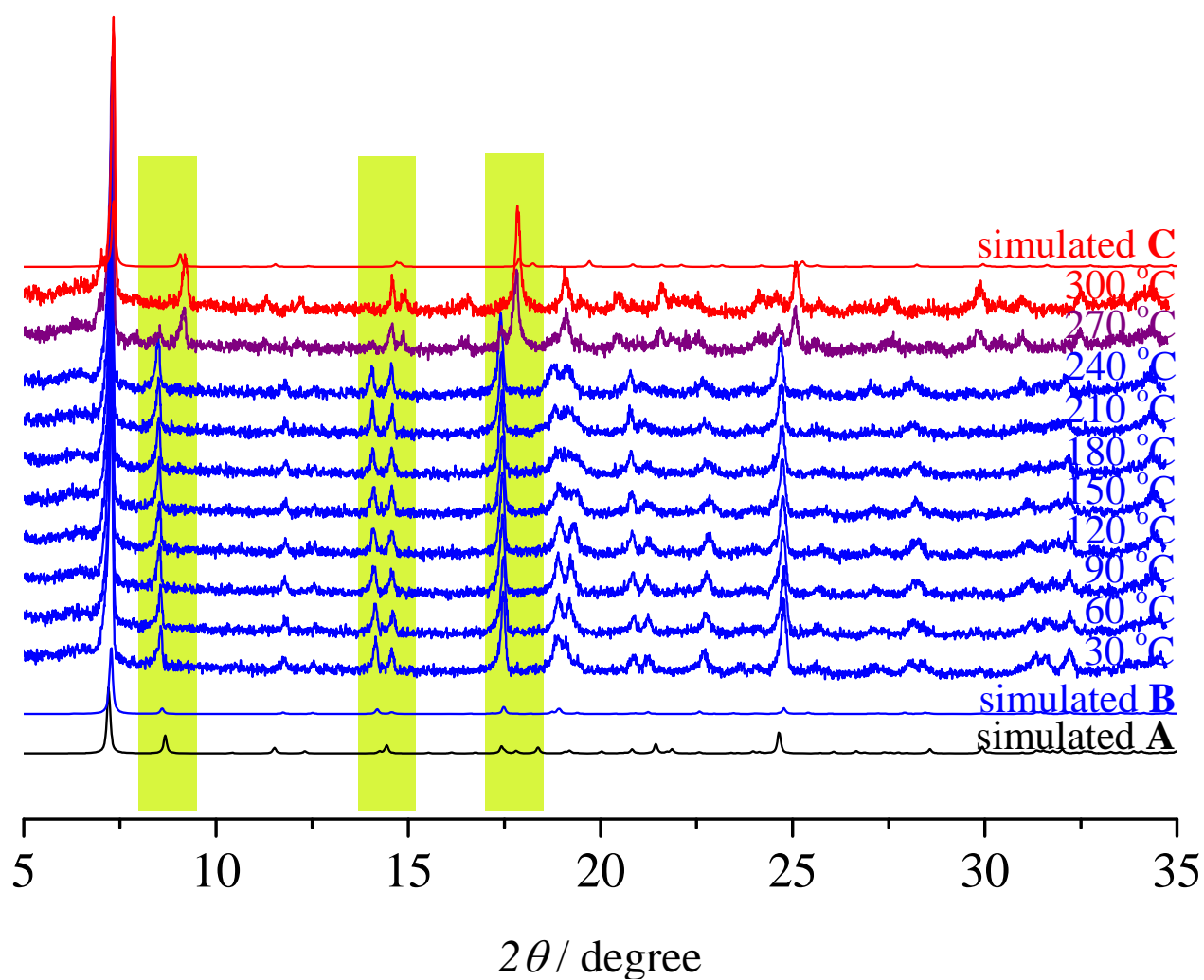**Figure S6.** Magnified Figure 2d.

Figure S7. Magnified Figure 2e.

simulated **C**
300 °C
270 °C
240 °C
210 °C
180 °C
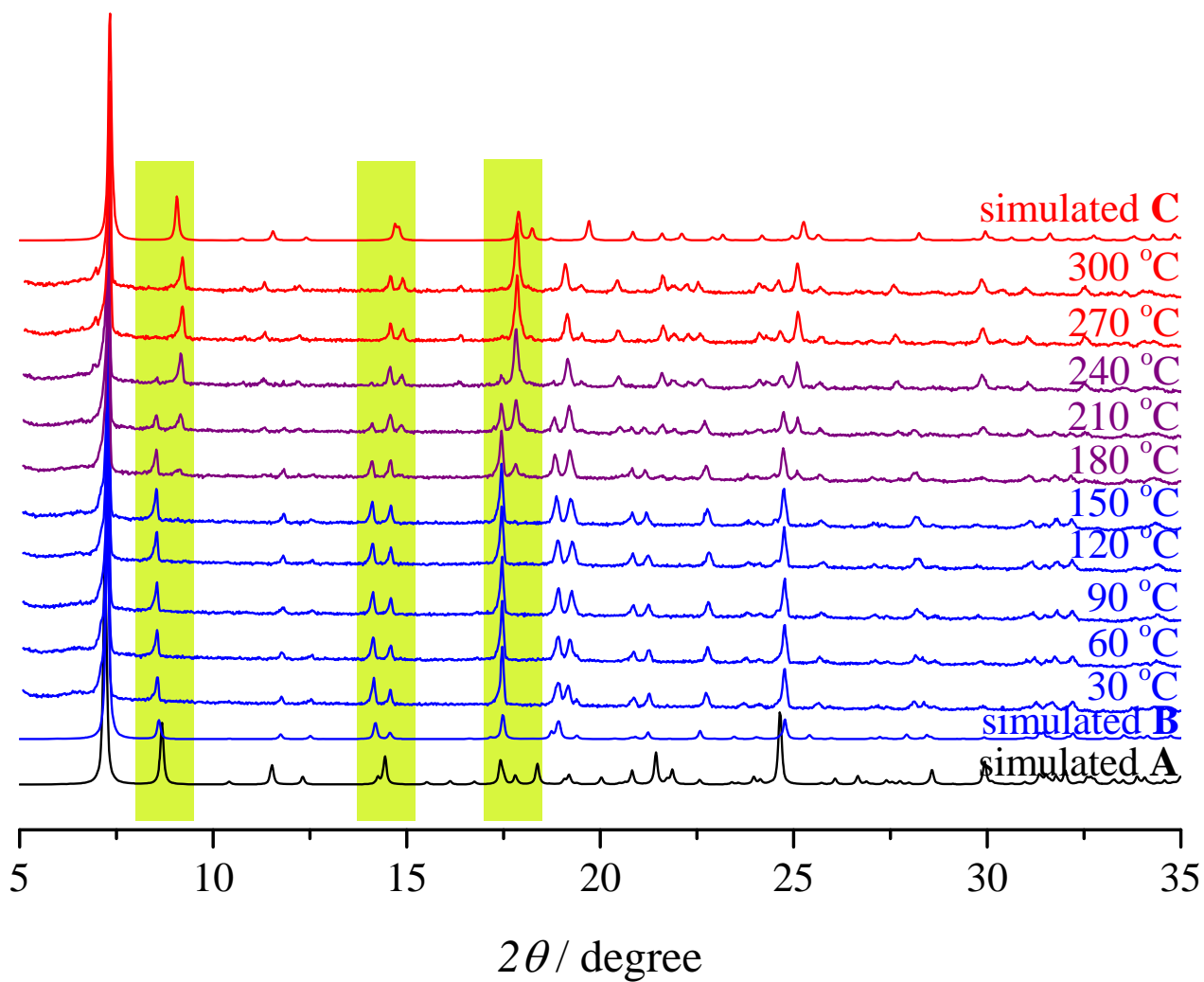150 °C
120 °C
90 °C
60 °C
30 °C
simulated **B**
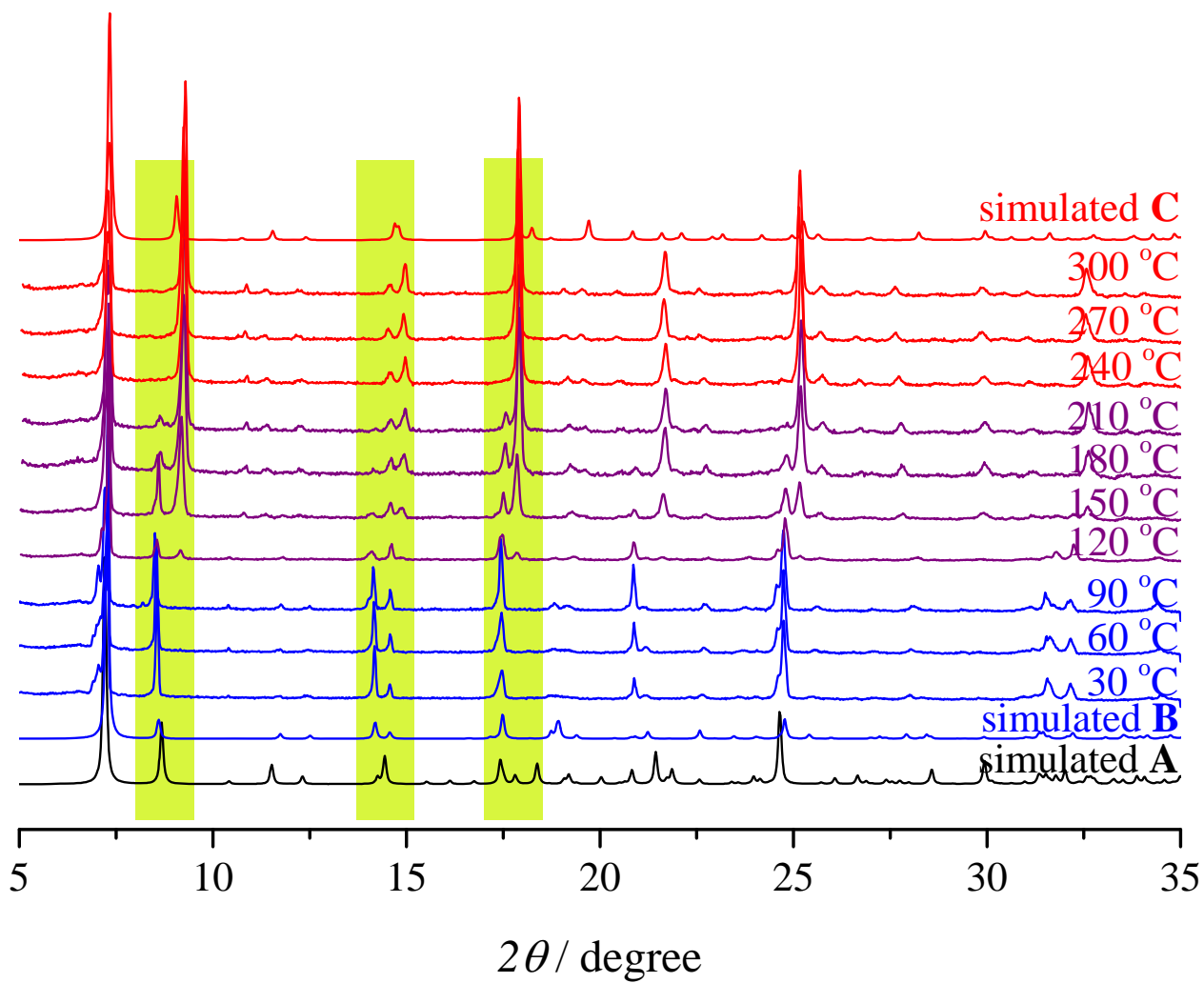simulated **A**

2θ / degree
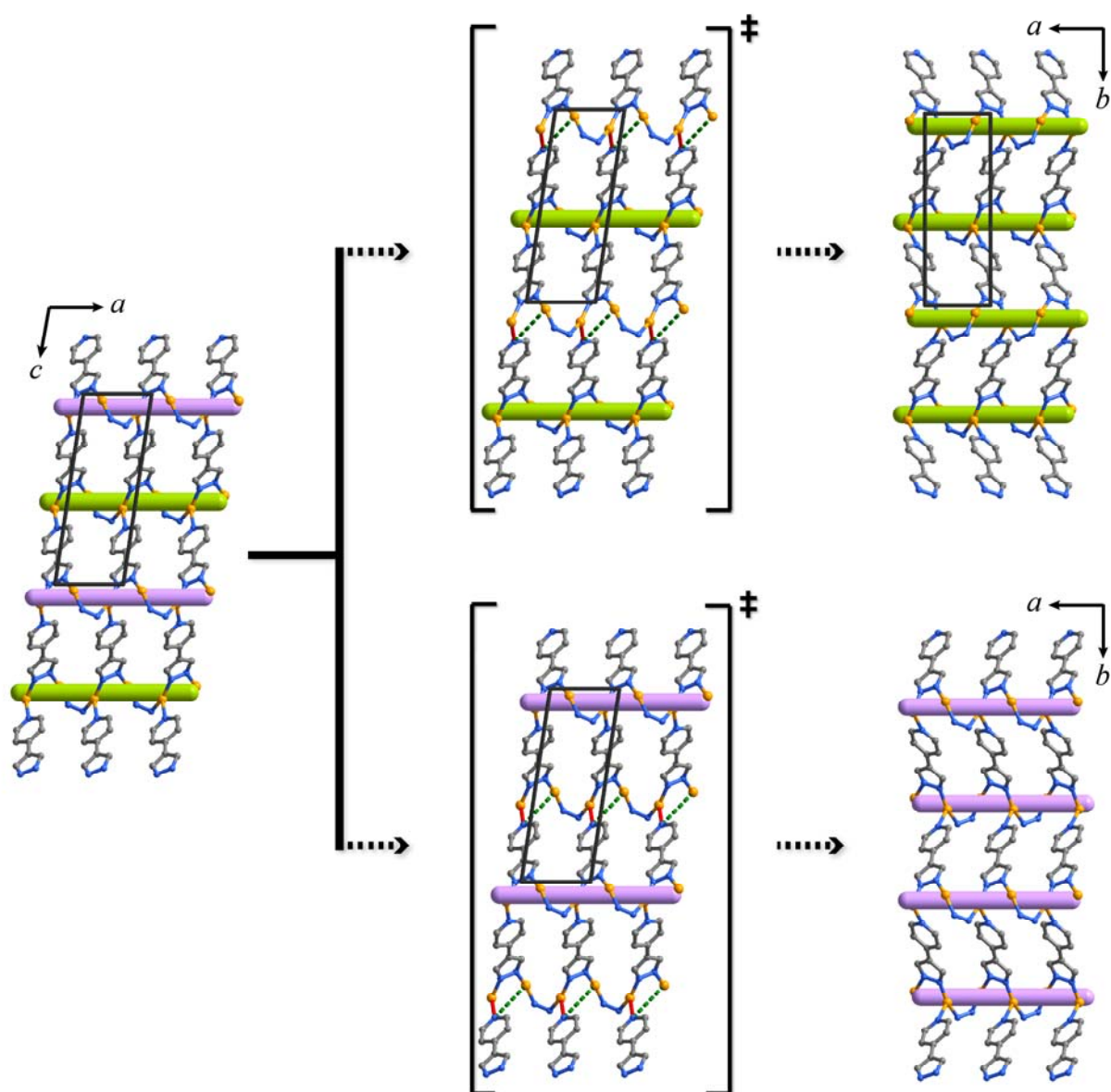
Figure S8. Magnified Figure 2f.

Figure S9. The full illustration of the proposed transformation mechanism from **B** to **C**.

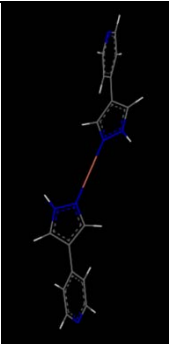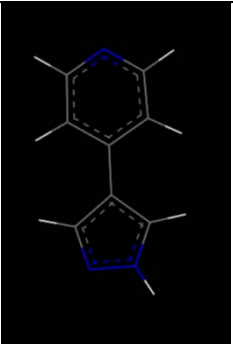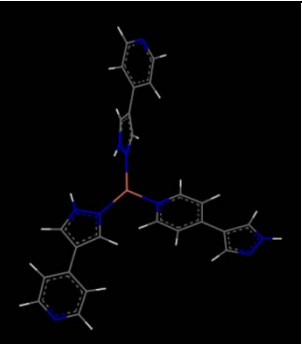| $E_1 = -1168.1218953$ Ha	$E_2 = -472.8931741$ Ha	$E_3 = -1641.0536590$ Ha
$\Delta E = E_1 + E_2 - E_3 = 101.3$ kJ/mol		

Figure S10. Optimized and energies of the structural fragments involved in the transformation from **B** to **C**.
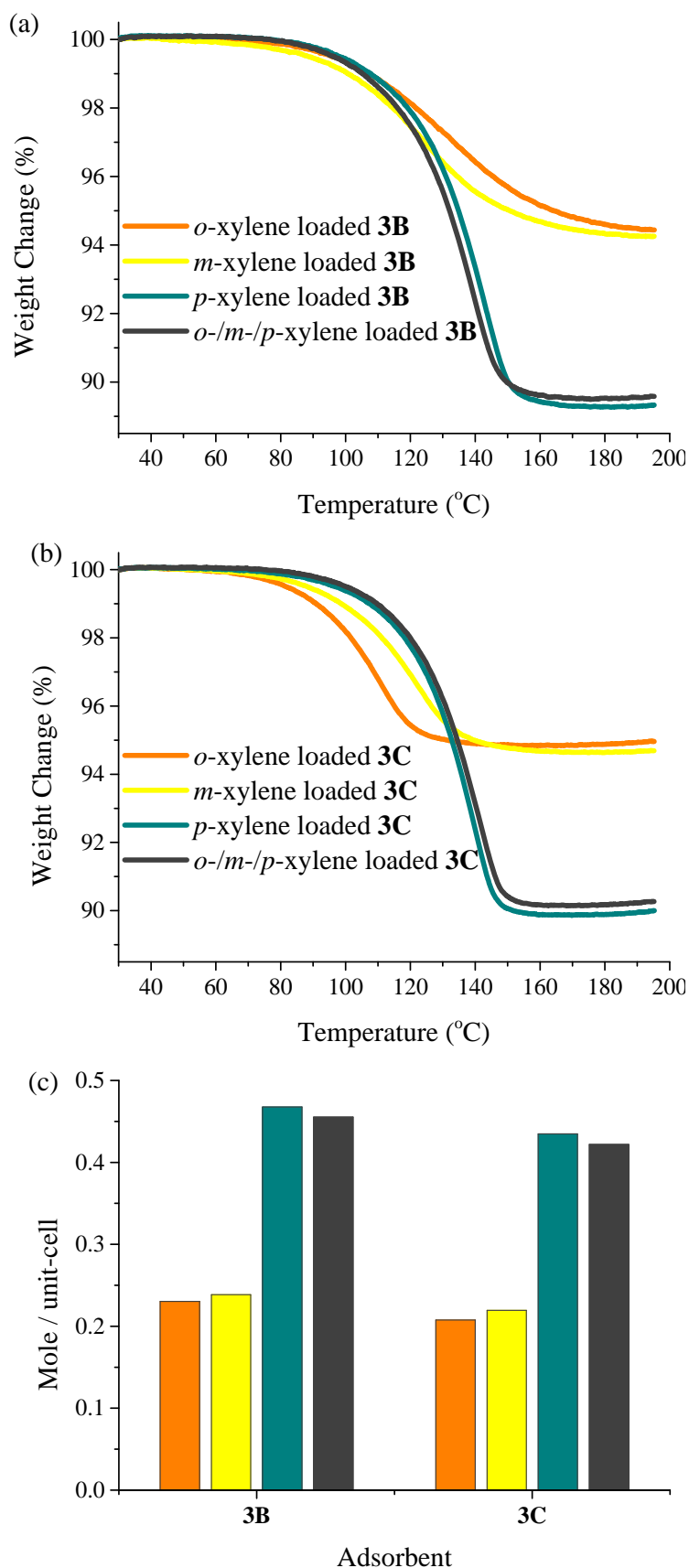
Figure S11. TG curves of (a) **3B** and (b) **3C** after adsorption of xylene isomers. (c) Summary of xylene uptakes. Colour scheme: *o*-xylene, orange; *m*-xylene, yellow; *p*-xylene, dark cyan; ternary xylene mixture, dark grey.
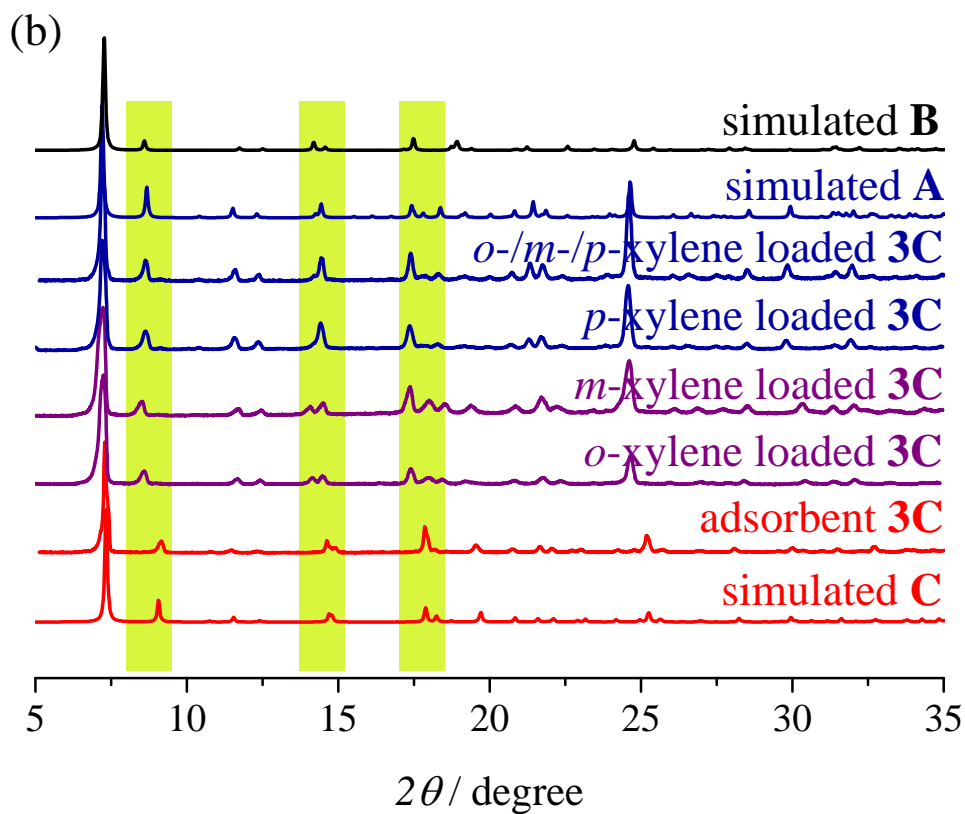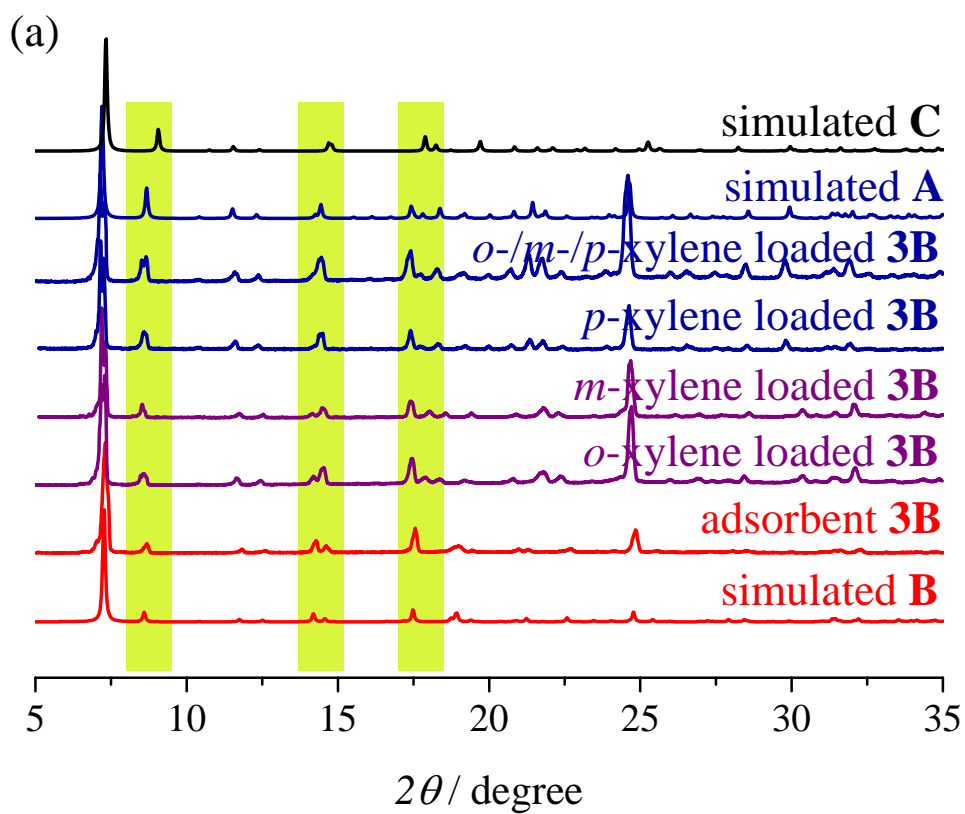
Figure S12. PXRD patterns of (a) **3B** and (b) **3C** after loaded with xylene isomers.
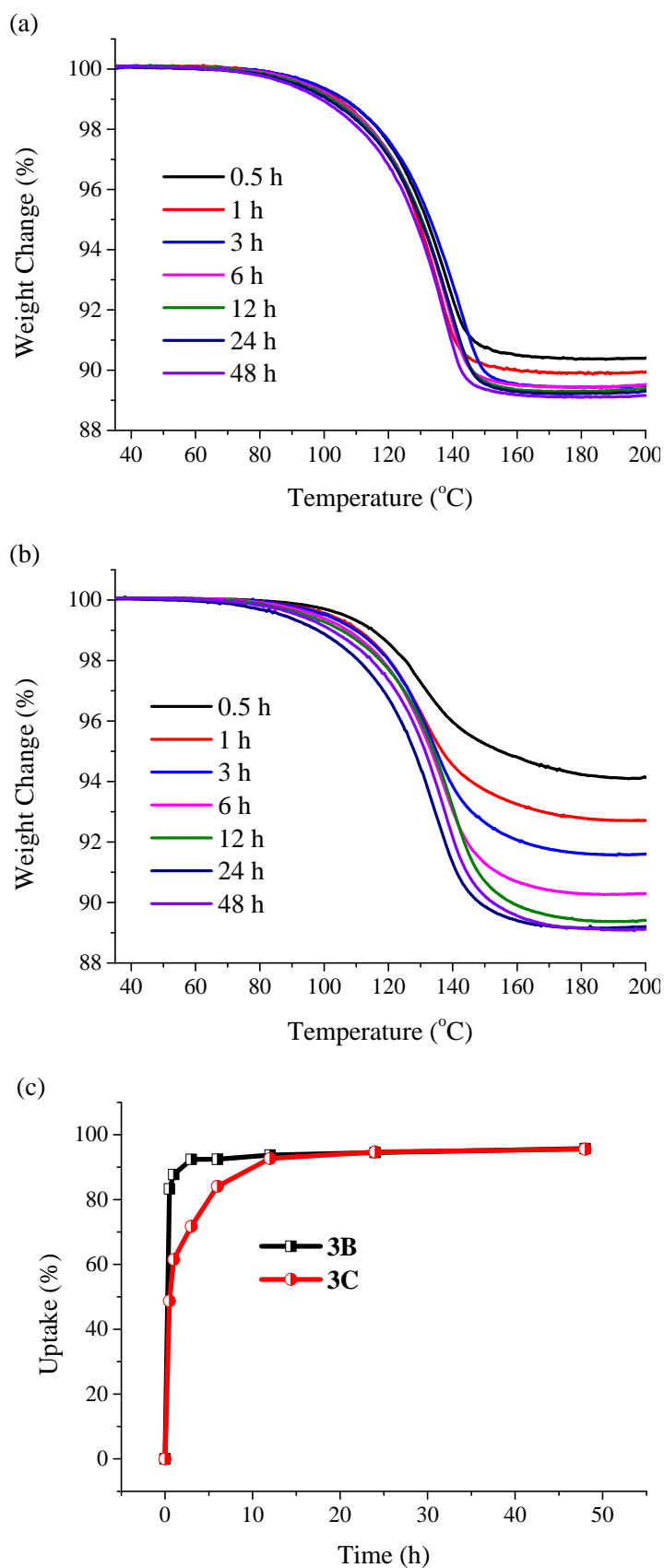
Figure S13. TG curves for (a) **3B** and (b) **3C** after immersion into equimolar mixture of xylene isomers for different times. (c) The corresponding adsorption kinetic profiles.
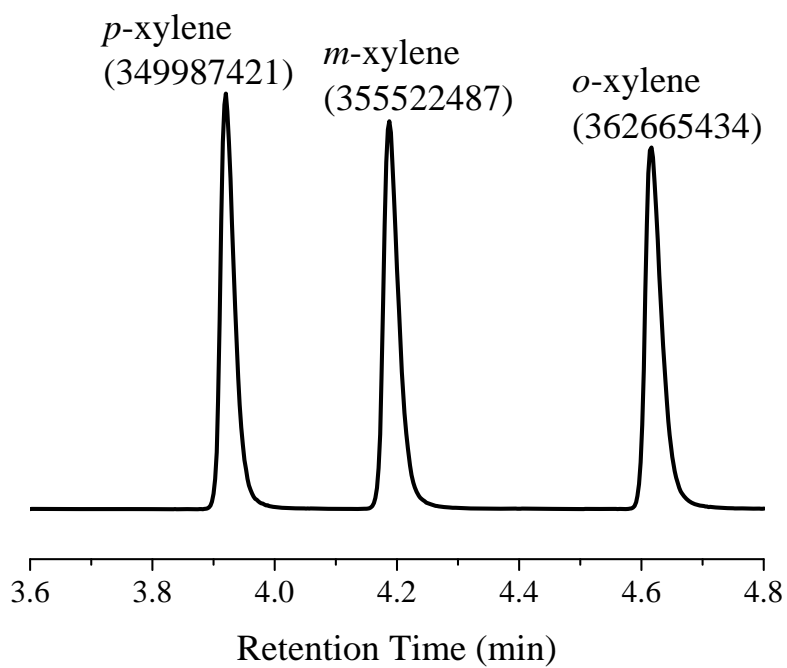
Figure S14. Gas chromatography curve of the *n*-heptane solution containing equimolar ternary mixture of xylene isomers. The integrated peak areas have been added in the parentheses above their corresponding peaks.

Figure S15. Xylene selectivities of **3B** in three consecutive ad-/desorption cycles. Gas chromatography curves of the digestion solutions of **3B** samples after immersed in equimolar mixture of xylene isomers in the (a) first, (b) second, and (c) third ad-/desorption cycle. Three parallel tests have been performed for each cycle. (d) Relative xylene isomer uptake in **3B** for three consecutive ad-/desorption cycles.
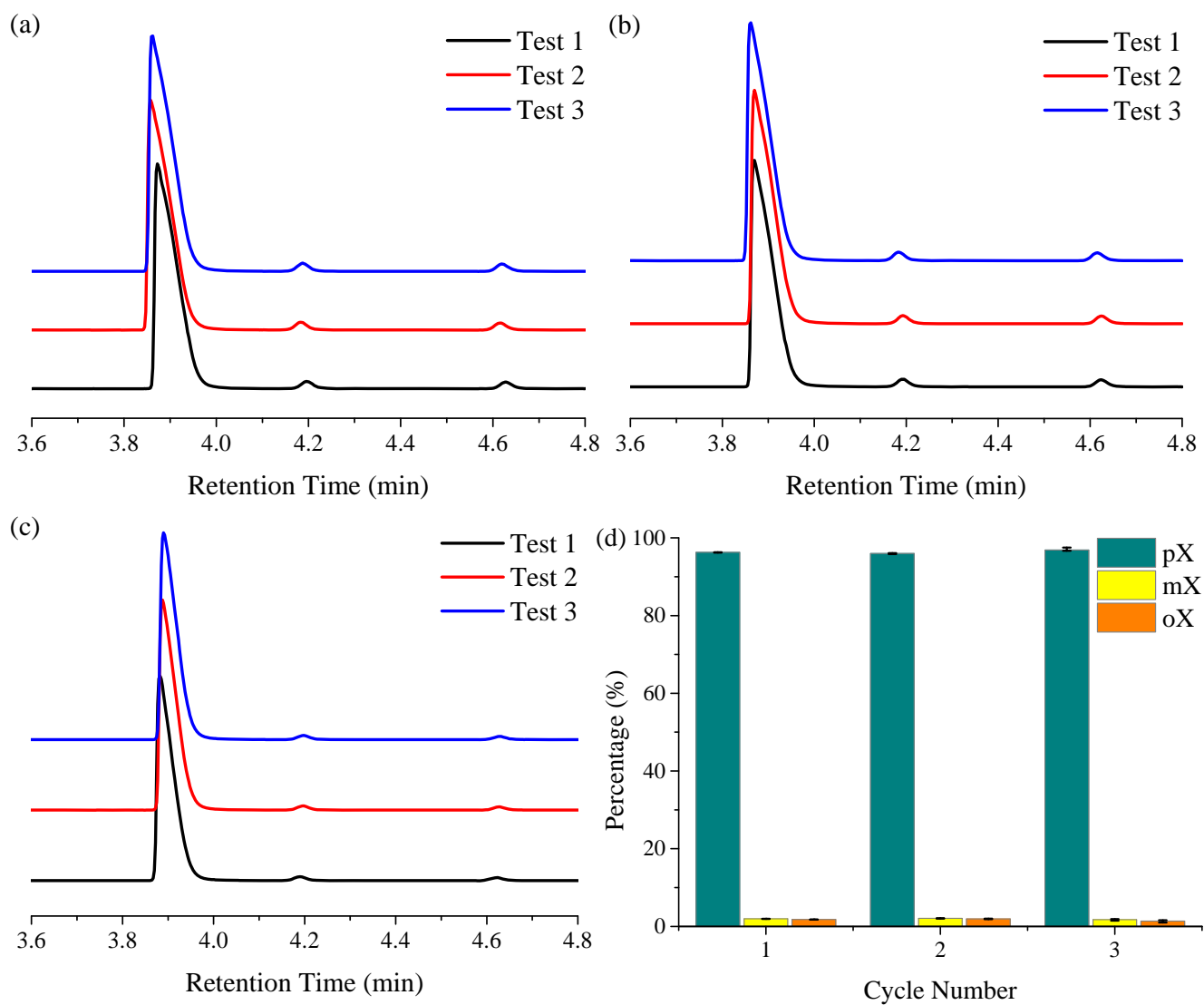
Figure S16. Xylene selectivities of **3C** in three consecutive ad-/desorption cycles. Gas chromatography curves of the solutions of **3C** samples after immersed in equimolar mixture of xylene isomers in the (a) first, (b) second, and (c) third ad-/desorption cycle. Three parallel tests have been performed for each cycle. (d) Relative xylene isomer uptake in **3C** for three consecutive ad-/desorption cycles.

Figure S17. TG curves for **1B** after immersed in equimolar mixture of xylene isomers for different times.

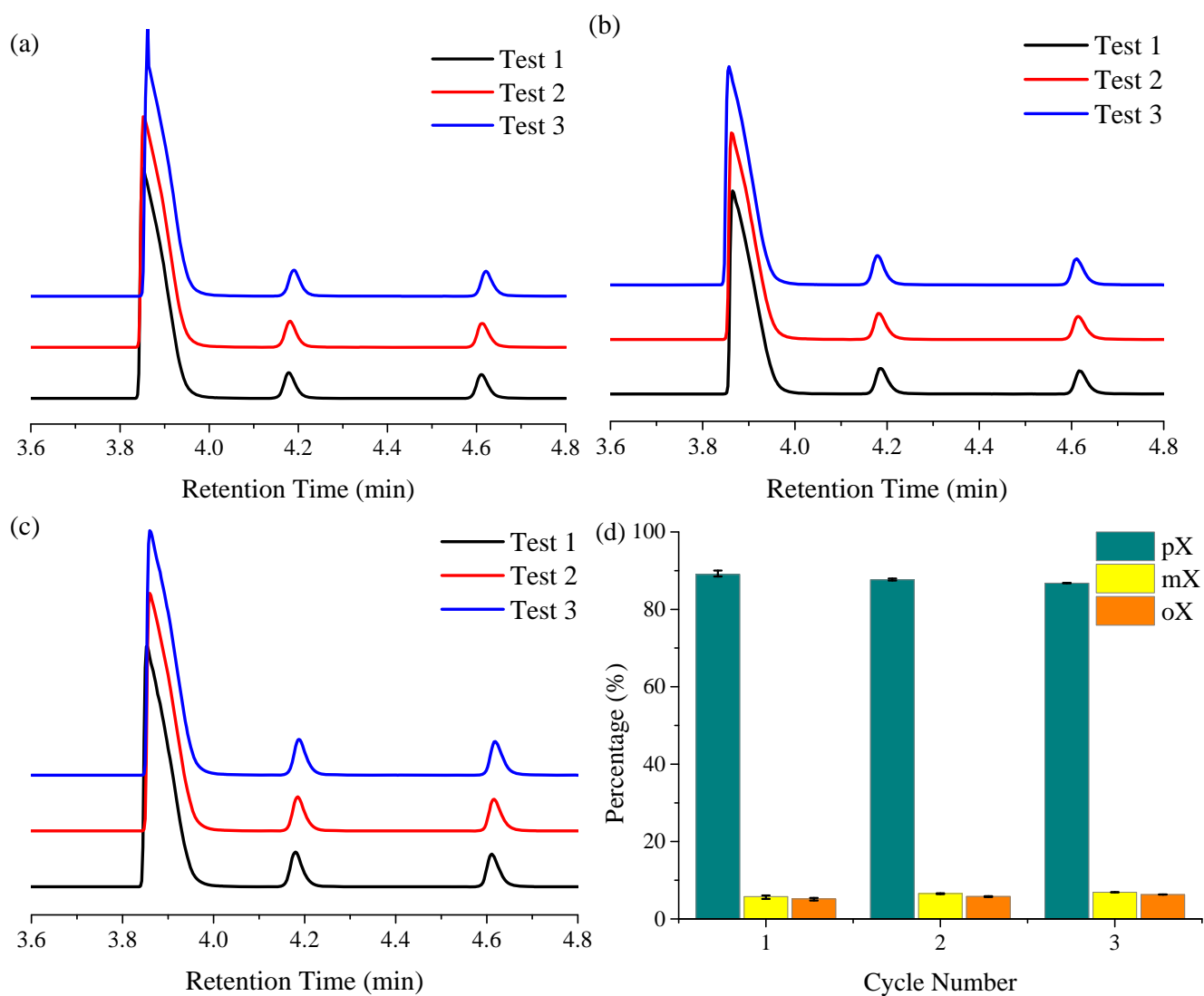**Figure S18.** Xylene selectivities of **1B** in three consecutive ad-/desorption cycles. Gas chromatography curves of the digestion solutions of **1B** samples after immersed in equimolar mixture of xylene isomers in the (a) first, (b) second, and (c) third ad-/desorption cycle. Three parallel tests have been performed for each cycle. (d) Relative xylene isomer uptake in **1B** for three consecutive ad-/desorption cycles.
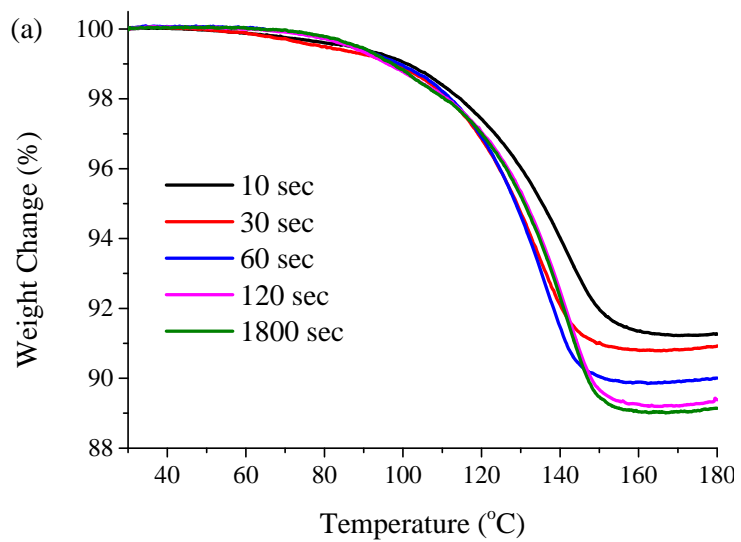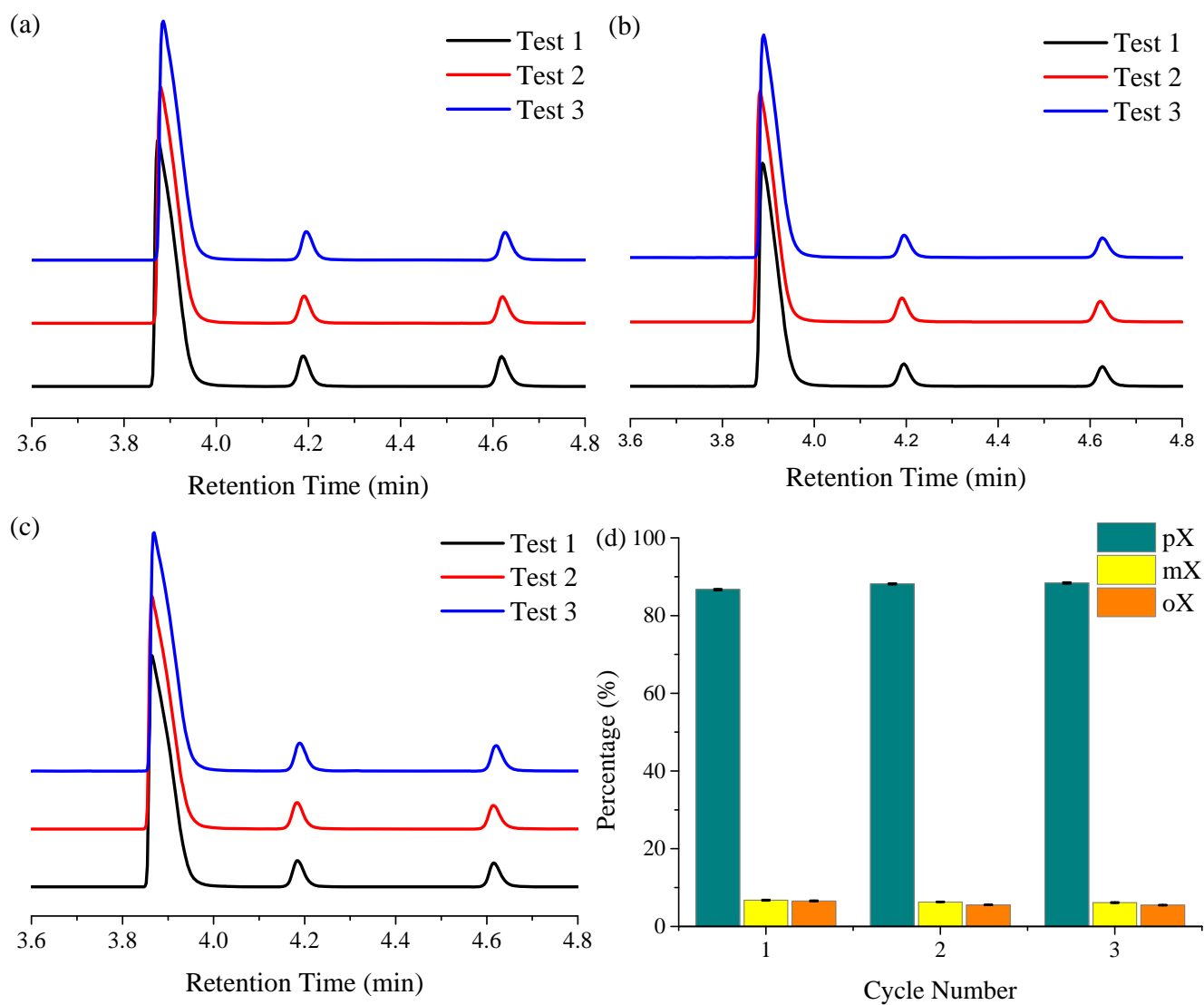
References

[1]   S. Tanaka, K. Fujita, Y. Miyake, M. Miyamoto, Y. Hasegawa, T. Makino, S. Van der Perre, J. Cousin Saint Remi, T. Van Assche, G. V. Baron, and J. F. M. Denayer, "Adsorption and diffusion phenomena in crystal size engineered ZIF-8 MOF," *J. Phys. Chem. C,* vol. 119, no. 51, pp. 28430-28439, 2015.

[2]   C. Zhang, J. A. Gee, D. S. Sholl, and R. P. Lively, "Crystal-size-dependent structural transitions in nanoporous crystals: adsorption-induced transitions in ZIF-8," *J. Phys. Chem. C,* vol. 118, no. 35, pp. 20727-20733, 2014.

[3]   S. Krause, V. Bon, I. Senkovska, D. M. Tobbens, D. Wallacher, R. S. Pillai, G. Maurin, and S. Kaskel, "The effect of crystallite size on pressure amplification in switchable porous solids," *Nat. Commun.,* vol. 9, no. 1, pp. 1573, 2018.

[4]   Y. Sakata, S. Furukawa, M. Kondo, K. Hirai, N. Horike, Y. Takashima, H. Uehara, N. Louvain, M. Meilikhov, T. Tsuruoka, S. Isoda, W. Kosaka, O. Sakata, and S. Kitagawa, "Shape-memory nanopores induced in coordination frameworks by crystal downsizing," *Science,* vol. 339, no. 6116, pp. 193-196, 2013.

[5]   N. Kavoosi, V. Bon, I. Senkovska, S. Krause, C. Atzori, F. Bonino, J. Pallmann, S. Paasch, E. Brunner, and S. Kaskel, "Tailoring adsorption induced phase transitions in the pillared-layer type metal-organic framework DUT-8(Ni)," *Dalton Trans.,* vol. 46, no. 14, pp. 4685-4695, 2017.

[6]   Sakaida, S., K. Otsubo, O. Sakata, C. Song, A. Fujiwara, M. Takata, and H. Kitagawa, "Crystalline coordination framework endowed with dynamic gate-opening behaviour by being downsized to a thin film," *Nat. Chem.,* vol. 8, no. 4, pp. 377-83, 2016.

[7]   J. S. Wright, I. J. Vitórica-Yrezábal, S. P. Thompson, and L. Brammer, "Arene selectivity by a flexible coordination polymer host," *Chem. Eur. J.,* vol. 22, no. 37, pp. 13120-13126, 2016.

[8]   J. Lannoeye, B. Van de Voorde, B. Bozbiyik, H. Reinsch, J. F. M. Denayer, and D. De Vos, "An aliphatic copper metal-organic framework as versatile shape selective adsorbent in liquid phase separations," *Micropor. Mesopor. Mater.,* vol. 226, pp. 292-298, 2016.

[9]   J. E. Warren, C. G. Perkins, K. E. Jelfs, P. Boldrin, P. A. Chater, G. J. Miller, T. D. Manning, M. E. Briggs, K. C. Stylianou, J. B. Claridge, and M. J. Rosseinsky, "Shape selectivity by guest-driven restructuring of a porous material," *Angew. Chem. Int. Ed.,* vol. 53, no. 18, pp. 4592-4596, 2014.

[10]   F. Vermoortele, M. Maes, P. Z. Moghadam, M. J. Lennox, F. Ragon, M. Boulhout, S. Biswas, K. G. Laurier, I. Beurroies, R. Denoyel, M. Roeffaers, N. Stock, T. Duren, C. Serre, and D. E. De Vos, "p-Xylene-selective metal-organic frameworks: a case of topology-directed selectivity," *J. Am. Chem. Soc.,* vol. 133, no. 46, pp. 18526-18529, 2011.

[11]   W. Huang, J. Jiang, D. Wu, J. Xu, B. Xue, and A. M. Kirillov, "A highly stable nanotubular MOF rotator for selective adsorption of benzene and separation of xylene isomers," *Inorg. Chem.,* vol. 54, no. 22, pp. 10524-10526, 2015.

[12]   Peralta, D., G. Chaplais, A. Simon-Masseron, K. Barthelet, C. Chizallet, A. A. Quoineaud, and G. D. Pirngruber, "Comparison of the behavior of metal-organic frameworks and zeolites for hydrocarbon separations," *J. Am. Chem. Soc.,* vol. 134, no. 19, pp. 8115-26, 2012.

[13]   J. A. Gee, K. Zhang, S. Bhattacharyya, J. Bentley, M. Rungta, J. S. Abichandani, D. S. Sholl, and S. Nair., "Computational identification and experimental evaluation of metal-organic frameworks for xylene enrichment," *J. Phys. Chem. C,* vol. 120, pp. 12075-12082, 2016.